



Research Article

Assessing the magnetic order dependent γ -surface of Cr-Co-Ni alloys

Zhibiao Yang^{a,b}, Song Lu^{b,*}, Yanzhong Tian^{c,*}, Zijian Gu^c, Huahai Mao^{d,e}, Jian Sun^{a,*}, Levente Vitos^{b,f,g}



^a Shanghai Key Laboratory of Advanced High-Temperature Materials and Precision Forming, School of Materials Science and Engineering, Shanghai Jiao Tong University, Shanghai 200240, China

^b Applied Materials Physics, Department of Materials Science and Engineering, Royal Institute of Technology, Stockholm SE-100 44, Sweden

^c Key Laboratory for Anisotropy and Texture of Materials (Ministry of Education), School of Materials Science and Engineering, Northeastern University, Shenyang 110819, China

^d Unit of Structures, Department of Materials Science and Engineering, KTH, SE-10044, Stockholm, Sweden

^e Thermo-Calc Software, Råsundav. 18, SE-16767, Solna, Sweden

^f Division of Materials Theory, Department of Physics and Materials Science, Uppsala University, P.O. Box 516, Uppsala SE-75120, Sweden

^g Research Institute for Solid State Physics and Optics, Wigner Research Center for Physics, Budapest H-1525, P.O.Box 49, Hungary

ARTICLE INFO

Article history:

Received 7 October 2020

Received in revised form 23 October 2020

Accepted 26 October 2020

Available online 24 December 2020

Keywords:

Cr-Co-Ni alloys

Stacking fault energy

Transformation-induced plasticity

Twinning-induced plasticity

Ab initio

ABSTRACT

In order to efficiently explore the nearly infinite composition space in multicomponent solid solution alloys for reaching higher mechanical performance, it is important to establish predictive design strategies using computation-aided methods. Here, using *ab initio* calculations we systematically study the effects of magnetism and chemical composition on the generalized stacking fault energy surface (γ -surface) of Cr-Co-Ni medium entropy alloys and show that both chemistry and the coupled magnetic state strongly affect the γ -surface, consequently, the primary deformation modes. The relations among various stable and unstable stacking fault energies are revealed and discussed. The present findings are useful for studying the deformation behaviors of Cr-Co-Ni alloys and facilitate a density functional theory based design of transformation-induced plasticity and twinning-induced plasticity mechanisms in Cr-Co-Ni alloys.

© 2021 Published by Elsevier Ltd on behalf of The editorial office of Journal of Materials Science & Technology. This is an open access article under the CC BY license (<http://creativecommons.org/licenses/by/4.0/>).

1. Introduction

High entropy alloys (HEAs) were originally proposed by Yeh and Cantor in 2004 [1,2] as equiatomic concentrated solid solutions, which stabilize the single-phase structure through the maximized configurational entropy. Based on this concept, many types of single-phase HEAs have been successfully developed and some of them have been demonstrated possessing excellent mechanical properties, including equiatomic CrCoNi medium entropy alloy (MEA) [3,4], CrFeCoNi [5,6] and CrMnFeCoNi [2,7,8] HEAs. Recent development in HEAs has lifted the restriction of entropy maximization in order to explore the vast composition space in these multicomponent alloys. In particular, Li et al. [9] proposed the so-called ‘metastability-engineering strategy’ in Cr-Mn-Fe-Co alloys to optimize the mechanical performance, which represents one

guideline of designing HEAs. The composition of the alloy was modified in order to trigger the transformation-induced plasticity (TRIP) [9,10] or the twinning-induced plasticity (TWIP) effects [11,12]. This design concept combines the benefits from the massive solid solution hardening in HEAs with the TRIP/TWIP effects. Following this idea, they have designed TRIP or TWIP assisted single- and dual-phase HEAs with intriguing mechanical properties in Cr-Mn-Fe-Co alloys [9,12]. In fact, MEAs/HEAs such as CrCoNi and CrMnFeCoNi are also strengthened by the TRIP and/or TWIP effects [3,4,7], the maximized configuration entropy however does not play critical roles on the mechanical performance. In particular, the CrCoNi MEA exhibits extraordinary combination of high strength, high ductility and high fracture toughness [3,4], superior to CrMnFeCoNi and any other investigated ternary or quaternary equiatomic variants. More interestingly, the mechanical properties of these HEAs are further improved at cryogenic temperatures, which are ascribed to the enhanced TRIP/TWIP effects via the occurrence of twin + hexagonal close packed (hcp) lamellar structure, partly due to the temperature effect on the stacking fault energy (SFE) [4].

* Corresponding authors.

E-mail addresses: songlu@kth.se (S. Lu), tianyanzhong@mail.neu.edu.cn (Y. Tian), jsun@sjtu.edu.cn (J. Sun).

Table 1

Calculated and experimental [6–68] SFEs for a series of ternary Cr-Co-Ni alloys at room temperature. The corresponding magnetic state as predicted in Fig. 1(a) is also listed.

Alloy	Magnetic state	γ_0^{fcc}	$\gamma_{\text{sf}}^{\text{fcc}}$	$\gamma_{\text{sf}}^{\text{exp.}}$
Cr ₁₀ Co ₅₀ Ni ₄₀	FM	−37	−17	34 [66]
Cr ₁₀ Co ₆₀ Ni ₃₀	FM	−50	−31	18 [66]
Cr ₁₅ Co ₅₅ Ni ₃₀ (T3)	FM	−55	−49	16 [66]
Cr ₁₅ Co ₅₀ Ni ₃₅ (T4)	FM	−45	−32	25 [66]
Cr ₁₅ Co ₄₅ Ni ₄₀ (T5)	FM	−27	−15	37 [66]
Cr ₁₅ Co ₄₀ Ni ₄₅ (T6)	FM	−12	−5	46 [66]
Cr ₂₀ Co ₂₀ Ni ₆₀	PM	18	37	71 [66]
Cr ₂₀ Co ₅₀ Ni ₃₀	PM	−45	−22	20 [66]
Cr ₂₅ Co ₁₀ Ni ₆₅	PM	15	35	71 [66]
Cr ₂₅ Co ₃₀ Ni ₄₅	PM	−10	12	50 [66]
Cr ₂₅ Co ₄₀ Ni ₃₅	PM	−20	0.5	41 [66]
Cr ₃₀ Co ₂₀ Ni ₅₀	PM	−18	3.5	43 [66]
Cr ₃₀ Co ₄₀ Ni ₃₀	PM	−58	−23	11 [66]
CrCoNi	PM	−48	−24	18 [67], 22 [68]
Cr ₄₀ Co ₁₅ Ni ₄₅	PM	−24	−9	30 [66]
Cr ₄₀ Co ₃₀ Ni ₃₀	PM	−56	−37	13 [66]

The primary deformation modes in face-centered cubic (fcc) metals and alloys, namely, martensitic phase transformation (MT), twinning (TW), and dislocation slip (SL), depend strongly on the size of the stacking fault energy (SFE) [13–15]. For the purpose of alloy design, the correlation between the SFE and the deformation modes offers a practical strategy through optimizing chemical composition and concentrations, providing that the SFE versus chemistry and concentration relations are precisely established [15,16]. The relationship between experimental SFE ($\gamma^{\text{exp.}}$) and the prevalent deformation mode has been investigated experimentally in many alloys including the medium/high-Mn TRIP/TWIP steels [15,16], TWIP HEAs (Cr₁₀Mn₄₀Fe₄₀Co₁₀ and CrMnFeCoNi) [12,17] and TRIP dual-phase HEAs (Cr₁₀Mn₃₀Fe₅₀Co₁₀) [9,10]. However, the relationship based merely on experimental SFE and its dependence on composition, especially when $\gamma^{\text{exp.}}$ is small [18], has a very limited predictive power. Our recent reconsideration of the experimental methods for determining the SFE shows that $\gamma^{\text{exp.}}$ is limited to positive values and cannot reflect the real thermodynamic stability of the fcc phase in metastable alloys like Co-rich Co-Ni alloys or CrCoNi-based HEAs [19]. Today, a complete and precise database of SFE in HEAs is still missing, particularly in multicomponent alloys with complicated magnetic phase diagram. In literature, there are a lot of activities focusing on developing non-equimolar HEAs [9,12,20]. In the CrCoNi-based system, composition may change from the Co-based alloys to Ni-based alloys, while keeping random solid solution with close-packed structures [21]. Already in this simple ternary case, there are nearly infinite ways to tune the composition, but a quantitative parameter to guide alloy design is still missing. Furthermore, depending on the nominal composition and temperature, the ternary alloys can be ferromagnetic (FM) or paramagnetic (PM). However, the influence of magnetic state on the SFE (as well as the γ -surface) and the primary deformation mechanisms remains unclear. Previous theoretical studies mostly adopt the nonmagnetic (NM) approximation for the PM state [22–24], which totally neglects the effects of the local magnetic moments [25] or use the spin-polarized calculations at 0 K [26] which produce complicated magnetic configurations depending on local atomic environments in the supercells.

Beyond the theoretical investigations focusing on nominal compositions, there are studies suggesting that the chemical short-range order (SRO) and local chemical fluctuation greatly affect the SFE and the γ -surface, and thus the deformation behavior and mechanical properties [27–30]. However, the precise role of SRO or chemical fluctuation and to which extent they can be tuned in the apparently random HEAs remains an open question awaiting for more experimental evidence [31]. Recent experiments demonstrated that after a solid-solution treatment the element

distributions in the CrCoNi and CrMnFeCoNi alloys were rather homogenous [7,32]. Additionally, when chemical fluctuations or SROs are present and affect the SFE, e.g., accelerated by high-temperature aging on purpose [30], one should also consider the magnetic effect that couples with the local chemical environment when studying the SFE, which are usually neglected in literature.

In the present work, we report a systematical *ab initio* study of the chemical and magnetic state dependence of the γ -surface of the fcc Cr_xCo_yNi_{100-x-y} ($10 \leq x \leq 45$, $10 \leq y \leq 60$, at.%) MEAs and explore their influence on the primary deformation mechanisms. We show the critical role played by magnetism on the γ -surface. The present findings will be useful for understanding how the prevalent deformation mechanism changes with composition during deformation and facilitate designing new TRIP or TWIP Cr-Co-Ni alloys.

2. Computational methods

First-principles calculations were performed by using the exact muffin-tin orbitals (EMTO) method based on density functional theory (DFT) [33–35]. The EMTO method is an improved screened Korringa-Kohn-Rostoker (KKR) method [36], where the one-electron potentials are represented by large overlapping muffin-tin potential spheres. Generalized gradient approximation (GGA) parameterized by Perdew, Burke and Ernzerhof (PBE) was used to treat the exchange-correlation density functional [37]. In the self-consistent calculations, the one-electron equations were solved within the soft-core scheme and scalar-relativistic approximation. The Green's function was calculated for 16 complex energy points distributed exponentially on a semi-circular contour, including states within 1 Ry below the Fermi level. The basis sets included s, p, d, and f orbitals. The Cr-3p⁶4s²3d⁴, Co-3p⁶4s²3d⁷, Ni-3p⁶4s²3d⁸ were treated as valence states. The irreducible parts of the Brillouin zones were sampled by uniformly distributed k -points. The k -mesh was carefully tested and the $12 \times 24 \times 3$ mesh was adopted for all calculations.

The chemical disorder was described with the coherent potential approximation (CPA) as implemented in the EMTO method [38]. CPA is an efficient and useful approach to treat the compositional and magnetic disorder in random solid-solution alloys. In the present study, we considered both FM and PM states. The PM state was simulated by the static disordered local moments (DLM) model [39], and possible thermal spin fluctuations were neglected [40]. Since we only considered temperature effects up to the room temperature, in the free energy $F(T,V)$ we included effects due to thermal lattice expansion and magnetic entropy for the PM state [35]. The electronic entropy and lattice vibrational terms were

neglected as their contributions to energy were found small up to the room temperature [25,41]. The equilibrium lattice parameters at the PM and FM states were obtained from the Morse-type of equation of state and the lattice parameters corresponding to temperature T were derived by using the experimental thermal lattice expansion coefficient of pure metals [42] in connection with rule of mixture. Namely, we took $\alpha_{\text{alloy}} = 1/n \sum_i^n \alpha_i$, where n is the number of elements and α_i the thermal lattice expansion coefficient of element i . According to the previous study [42], the calculated thermal lattice expansion coefficients show a good agreement with the experimental values for the MEAs around room temperature. For the sake of comparison, the calculations for the PM and FM states were carried out adopting the same thermal expansion coefficient.

The generalized stacking fault energy surface (GSFE, γ -surface) was determined by a rigid shift of one part of the fcc structure along the $1/6<11\bar{2}>$ direction in the $\{111\}$ slip planes following the method in Ref. [43]. The calculations were performed using a supercell containing 12 fcc $\{111\}$ layers with the stacking sequence of ABCABCABCABC for the fcc structure. The intrinsic stacking fault energy (ISF, $\gamma_{\text{isf}}^{\text{fcc}}$), unstable stacking fault energy (USF, $\gamma_{\text{usf}}^{\text{fcc}}$) and unstable twining fault energy (UTF, $\gamma_{\text{utf}}^{\text{fcc}}$) were extracted from the GSFE curve. The hexagonal close-packed (hcp) lattice was modeled by a similar supercell corresponding to ABABABABABAB packing.

3. Results

3.1. Magnetic phase diagram of ternary Cr-Co-Ni alloys

Some Cr-Co-Ni-based HEAs exhibit excellent mechanical properties at cryogenic temperatures [3,44], which are related to the underlying deformation mechanisms activated/enhanced at low temperatures. Since magnetism is strongly temperature dependent, first we estimate the magnetic phase diagram of ternary Cr-Co-Ni alloys.

In binary Ni-Cr alloys, the magnetic transition temperature (Curie temperature, T_c) decreases almost linearly from 627 K for pure Ni to zero for Cr concentration higher than ~13 at.% [45], while in binary Ni-Co alloys, T_c increases linearly with Co addition [46]. This can be understood considering that Cr atoms prefer antiferromagnetic coupling with each other and with Ni atoms, and thus magnetic frustrations lead to the reduction of magnetic moments and decreased T_c with increasing Cr concentration. On the other hand, Co couples ferromagnetically with Ni, which causes the increase in T_c with Co addition.

The composition dependent T_c can be estimated using the *ab initio* exchange interactions in combination with Monte-Carlo simulations based on Heisenberg Hamiltonia. Alternatively, one can make use of the mean-field approach, $T_c = 2/3(E_{\text{PM}} - E_{\text{FM}})/k_B$, where $E_{\text{PM}} - E_{\text{FM}}$ is the total energy difference between the PM and FM states calculated at the 0 K equilibrium state, and k_B is the Boltzmann constant [47]. Similar approach was adopted for calculating T_c in other HEAs [48,49]. The obtained T_c map as function of composition in ternary Cr-Co-Ni alloys is shown in Fig. 1(a). One finds that T_c decreases remarkably with increasing Cr and/or decreasing Co concentrations, which is consistent with their effects in the binary alloys. The rapid recession of ferromagnetism with increasing Cr concentrations is due to magnetic frustration [32,50]. The spins of Cr atoms prefer antiparallel alignment with neighboring Cr, Co and Ni spins, which cannot be satisfied on a fcc lattice. Consequently, both magnetic moments and T_c decrease. In the low-Cr and high-Co corner ($x \leq 15$, $y \geq 27$), T_c is above room temperature (RT), indicating the preferred FM state at ambient conditions. The FM region extends towards the low-Co and low-Cr region when decreasing temperature, e.g., at 77 K. It is worth to note that the equiatomic CrCoNi MEA has a very low T_c (~ 30 K), which is in

line with the magnetic measurement showing no magnetic order down to 2 K [32]. To further benchmark our T_c results, we compare the theoretical T_c with the experimental values [50] for ternary $\text{Cr}_x\text{Co}_{(100-x)/2}\text{Ni}_{(100-x)/2}$ ($20 \leq x \leq 30$) alloys in Fig. 1(b). It shows that the present mean-field approach overestimates T_c by ≤ 50 K at high Cr concentrations. The deviation is related to the quantum critical behavior as discussed by Sales et al. [32,50] since these alloys with high Cr concentrations are in the vicinity of the quantum critical region, which are not considered by the present DFT methods. Additionally, the mean-field approach often leads to overestimation of magnetic transition temperature [48,49]. Nevertheless, for the purpose of the present work, such level of accuracy in T_c is acceptable.

3.2. Phase stability and stacking fault energy

In binary Ni-Co alloys, the experimental determined fcc/hcp phase boundary at room temperature locates approximately at ~33 at.% Ni with wide a thermal hysteresis of the transformation process [46]. In binary Ni-Cr alloys, high Cr concentration promotes the formation of intermetallic σ and body-centered cubic (bcc) phases [51]. In binary Co-Cr alloys, maximum ~45 at.% Cr can be dissolved in fcc Co at ~1500 K [52]. For the ternary Cr-Co-Ni alloys, the equilibrium phase diagram at high temperatures is well documented [21], and the single fcc phase is likely to be obtained for the composition range studied here at high temperatures. However, the equilibrium phase diagram at ambient and cryogenic temperatures is not properly established, particularly for the phase stability relevant to the TRIP effect, i.e., fcc (γ) vs. bcc (α) or fcc vs. hcp (ε) phases. Further, the martensitic transformations are strongly affected by hydronic pressure [53,54] or applied stress [4,20], which cumbers experimental measurements for such properties. For example, deformation induced martensitic transformation in binary Co-Ni alloys was demonstrated highly dependent on the applied shear stress [13]. In CrCoNi-based HEAs, Zhang et al. [53] and Tracy et al. [54] showed that under pressure equiatomic CrMnFeCoNi can transform from fcc to hcp at room temperature and similar observations were obtained for equiatomic CrCoNi and CrFeCoNi [55].

In the following, we first assess the free energy differences ($\Delta F_{\text{fcc}-\text{bcc}} = F_{\text{bcc}} - F_{\text{fcc}}$ and $\Delta F_{\text{hcp}-\text{bcc}} = F_{\text{bcc}} - F_{\text{hcp}}$) between the α , γ and ε phases at 300 K. We find that both $\Delta F_{\text{fcc}-\text{bcc}}$ and $\Delta F_{\text{hcp}-\text{bcc}}$ are positive for all compositions studied here, indicating that the α phase is the least stable one. This is in line with previous experimental studies that no α phase has yet been found in the Cr-Co-Ni based MEAs and HEAs, which is different as compared to the Fe-Mn TRIP steels [56]. Similarly, in the Co-rich alloys (e.g., Co-(14–30)Cr-7.5Fe-7Mn-7.5Ni, at.%) α phase was also found unstable by both thermodynamic and *ab initio* calculations, which was further confirmed by experiments [57]. Thereby, for the purpose of studying the deformation behavior of fcc ternary Cr-Co-Ni alloys, the α phase is no further considered in the present work.

In order to explore the composition dependent driving force for the structural transformation, we show the area-scaled free energy difference ($\Delta F_{\text{fcc}-\text{hcp}} = F_{\text{hcp}} - F_{\text{fcc}}$) between the hcp and fcc phases, $\gamma_0^{\text{fcc}} = 2\Delta F_{\text{fcc}-\text{hcp}}/A$, for both FM and PM states, in Fig. 2(a) and (b), respectively. According to the thermodynamic expression of the SFE [58], $\gamma_{\text{isf}}^{\text{fcc}} = \gamma_0^{\text{fcc}} + 2\sigma$, where σ is the fcc/hcp interfacial energy in the magnitude of several mJ/m^2 [59], γ_0^{fcc} is usually considered as the first order approximation of $\gamma_{\text{isf}}^{\text{fcc}}$ and a direct indicator of the thermodynamic stability of the fcc phase with respect to the hcp one [60]. Therefore, negative γ_0^{fcc} means that the ε phase is energetically more stable than the γ phase. For both magnetic states, γ_0^{fcc} decreases with Co and Cr addition. Interestingly, Cr is found to be a stronger hcp stabilizer than Co, despite

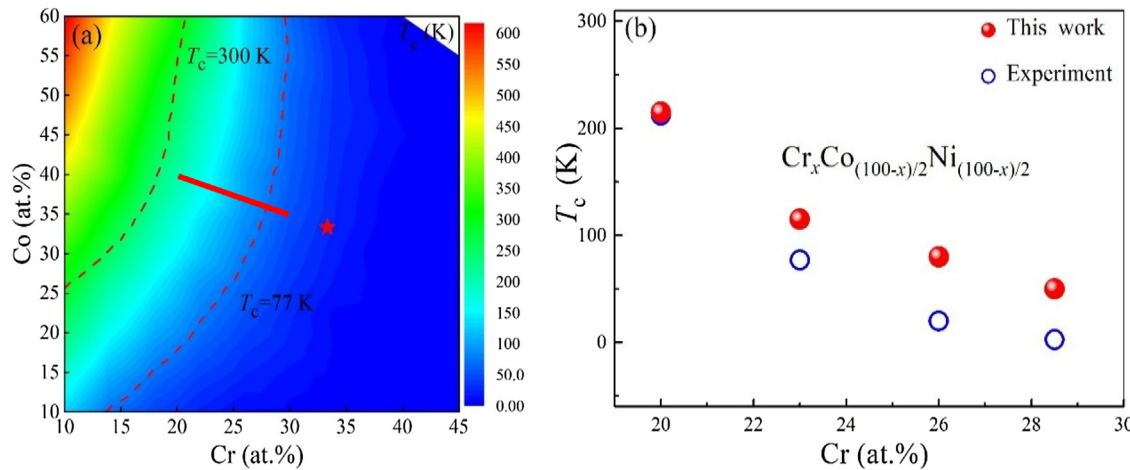


Fig. 1. (a) The composition dependent T_c in the ternary $\text{Cr}_x\text{Co}_y\text{Ni}_{100-x-y}$ ($10 \leq x \leq 45$, $10 \leq y \leq 60$) ternary alloys. The T_c of 300 K and 77 K are marked as dash lines. The position of the CrCoNi MEA is shown as a red star. (b) The calculated T_c with respect to Cr concentration in the ternary $\text{Cr}_x\text{Co}_{(100-x)/2}\text{Ni}_{(100-x)/2}$ ($20 \leq x \leq 30$) alloys (indicated by the solid line in (a)), compared to the available experimental data [50].

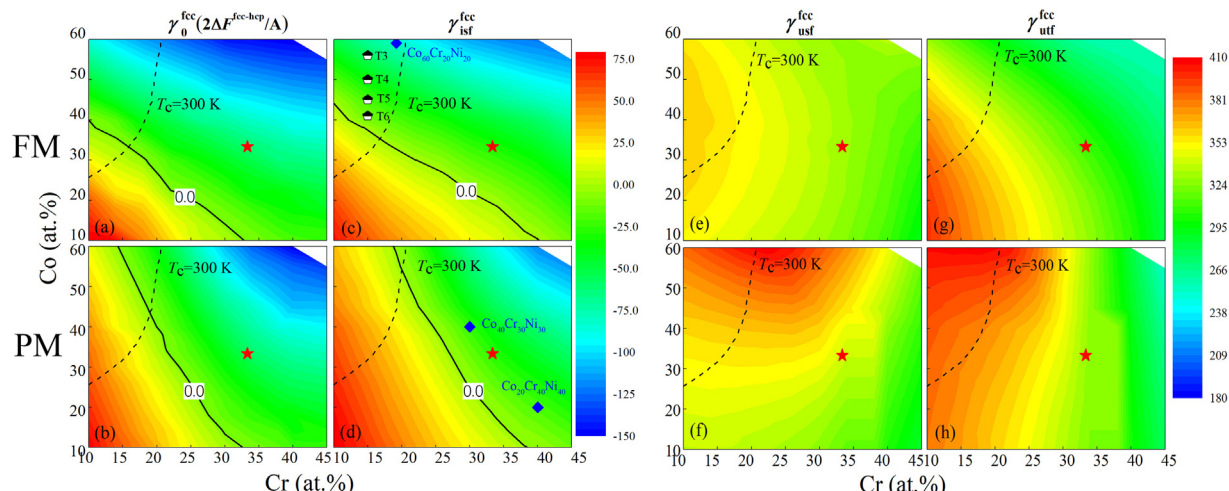


Fig. 2. The calculated γ_0^{fcc} , $\gamma_{\text{isf}}^{\text{fcc}}$, $\gamma_{\text{usf}}^{\text{fcc}}$ and $\gamma_{\text{utf}}^{\text{fcc}}$ for ternary $\text{Cr}_x\text{Co}_y\text{Ni}_{100-x-y}$ ($10 \leq x \leq 45$, $10 \leq y \leq 60$) alloys as a function of Cr and Co concentrations for FM (a, c, e, g) and PM states (b, d, f, h). Results are obtained at the room temperature. The T_c of 300 K is marked by dash lines. The solid lines represent zero values of γ_0^{fcc} and $\gamma_{\text{isf}}^{\text{fcc}}$ in (a-d). The position corresponding to the CrCoNi MEA is indicated by a red star. Available experimental results in ternary alloys are from Refs. [13,65].

that pure Cr is a B2 (bcc like) metal while Co is an hcp metal at ambient conditions. At room temperature, the γ phase is stable in the low-Co and low-Cr corner, and the ε phase is stable in the high-Co and high-Cr region. It is important to notice that for low Co concentration, the γ/ε phase boundaries (indicated by the solid line in Fig. 2(a) and (b)) at both FM and PM states are similar; while for high Co concentration, the boundary is shifted toward the high Cr direction at the PM state compared to that at the FM one, which may have a similar magnetic origin as in pure Co [61,62]. The previous studies showed that the ground state of Co is stabilized by magnetic order; and that phonon entropy, spin fluctuations and reduced magnetization all play important roles in the tendency to restore the fcc structure at high temperatures [61,62]. Actually, magnetism has been shown to strongly influence the phase stability in the Cr-Co-Ni-based HEAs as well [63,64]. For instance, Niu et al. [63] showed that the hcp phase of the CrCoNi MEA is more stable than the fcc one at both magnetic and non-magnetic states; while for the CrMnFe-CoNi HEA, spin-polarized calculations show that the magnetically frustrated Mn atoms reduce the fcc-hcp energy difference, compared to the hypothetical NM case. The present results and those in the above references highlight the importance of magnetism in studying the phase stability as well the deformation mechanisms

in alloys composed of 3d magnetic elements, e.g. Cr, Mn, Fe, Co and Ni.

The room-temperature $\gamma_{\text{isf}}^{\text{fcc}}$ maps are shown in Fig. 2(c) and (d) for the FM and PM states, respectively. They correlate nicely with the γ_0^{fcc} maps at the corresponding magnetic state (Fig. 3). The deviation between γ_0^{fcc} and $\gamma_{\text{isf}}^{\text{fcc}}$ in fact indicates the interfacial energy σ . Moreover, the linear dependence between γ_0^{fcc} and $\gamma_{\text{isf}}^{\text{exp}}$ confirm that the present theory captures the right trend of the thermal stability of the fcc phase in the ternary Cr-Co-Ni alloys. Using the calculated data of γ_0^{fcc} and $\gamma_{\text{isf}}^{\text{fcc}}$, the interfacial energy σ for the present alloys is estimated to be in the range of 2–8.5 mJ/m² according to $\sigma = (\gamma_{\text{isf}}^{\text{fcc}} - \gamma_0^{\text{fcc}})/2$, which agrees well with the previous theoretical values, e.g., 4–9 mJ/m² for CrCoNi MEA and CrMnFeCoNi HEA [69], 7.5–9 mJ/m² for ternary Fe-Cr-Ni alloys [59]. It is worth noting that in the present alloys, σ is mostly positive, indicating that it is possible to have small positive $\gamma_{\text{isf}}^{\text{fcc}}$ when the fcc structure is already thermodynamically unstable ($\gamma_0^{\text{fcc}} < 0$). We mention that from structural point of view, σ is the interfacial energy for the coherent interface composed of close-packed fcc{111} and hcp{0001} atomic planes, which is expected to be small and can have positive or negative values [59].

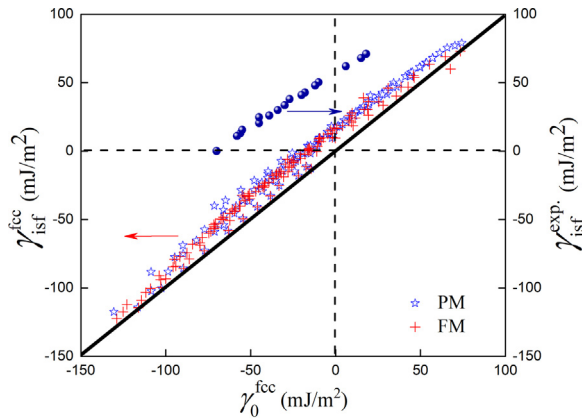


Fig. 3. Correlation between γ_0^{fcc} and $\gamma_{\text{isf}}^{\text{fcc}}$ in ternary Cr-Co-Ni alloys at both PM and FM states. Available experimental SFEs at room temperature [13,66–68] are also potted for comparison (values are listed in Table 1).

From Fig. 2, one can quantitatively calculate the chemistry dependence of the SFE, e.g., $\frac{\partial \gamma_{\text{isf}}^{\text{fcc}}}{\partial c_{\text{Cr}}} |_{c_{\text{Co}}}$ and $\frac{\partial \gamma_{\text{isf}}^{\text{fcc}}}{\partial c_{\text{Co}}} |_{c_{\text{Cr}}}$ at fixed Co or Cr concentrations. For instance, at 10 at.%, the typical $\frac{\partial \gamma_{\text{isf}}^{\text{fcc}}}{\partial c_{\text{Co}}} |_{c_{\text{Cr}}}$ and $\frac{\partial \gamma_{\text{isf}}^{\text{fcc}}}{\partial c_{\text{Cr}}} |_{c_{\text{Co}}}$ at the FM state are calculated to be approximately -2.0 mJ/m^2 per at.% Co and -2.4 mJ/m^2 per at.% Cr, respectively; while at the PM state, they are -1.2 and -3.2 mJ/m^2 , respectively. The present trends are in accordance with the previously reported trends in both experimental and theoretical estimates [66,70–73]. Specifically, for the CrCoNi MEA, the calculated SFE is -24 mJ/m^2 for the PM state and -29 mJ/m^2 for the FM state, respectively. These values are consistent with the previous theoretical results at the fully random state, e.g., -18 mJ/m^2 [23], -24 mJ/m^2 [22] and -43 mJ/m^2 [27].

We mention here that one cannot directly compare the theoretical SFE with the experimental values, e.g., $18 \pm 4 \text{ mJ/m}^2$ [67] and

$22 \pm 4 \text{ mJ/m}^2$ [68]. The latter ones are usually determined from the partial dislocation separations (d) [74] and they are restricted to be positive as decided by the $\gamma_{\text{isf}}^{\text{exp}} \propto \frac{1}{d}$ relationship. Furthermore, in metastable alloys, in response to external stress, dislocations are easily separated into wide SF ribbons, even at very small strains [75], and therefore, it is not a trivial task to measure the partial separation d [70]. Smith et al. [76] measured the partial separation of the $a/2<110>\{111\} 60^\circ$ mixed dislocations in the CrMnFeCoNi HEA and found significantly large variations in d . Similarly, Qi et al. [77] also reported that the width of the SF ribbon in 60° dislocations is distributed in the range of $3.8\text{--}11.3 \text{ nm}$, resulting in a wide distribution of the experimental SFE, $15.5\text{--}46.2 \text{ mJ/m}^2$ in $\text{Fe}_{42}\text{Mn}_{38}\text{Co}_{10}\text{Cr}_{10}$ HEA. For more discussion regarding the experimental determination of the SFE, the readers are referred to Ref. [19].

One notices that for the equiatomic CrCoNi MEA, the $\gamma_{\text{isf}}^{\text{fcc}}$ values obtained at various magnetic states (NM [22,23], PM and FM in the present work) do not differ significantly. This is likely because the local PM moments for the CrCoNi MEA nearly vanish (Fig. 4). At the FM state, the atomic magnetic moments obtained with the current CPA for the treatment of solid solution agree well with the previous supercell results. For example, Niu et al. [63] showed that spin-polarized and non-spin-polarized supercell calculations result in similar SFE for the CrCoNi MEA. The obtained atomic magnetic moments show quite fluctuations influenced by the local chemical environments, but the averaged values nice agree with the present ones. This observation justifies the previously adopted NM approximation for the PM CrCoNi MEA alloy at room temperature [22,23]. However, for the alloys with high-Co and low-Cr contents, $\gamma_{\text{isf}}^{\text{fcc}}$ differs significantly at different magnetic states, which is related to the large magnetic moments for the FM state, comparing to the almost vanished ones for the PM state (Fig. 4). Additionally, in CrMnFeCoNi, it was demonstrated that Mn causes strong magnetic frustration in spin-polarized calculations, which eliminates the fcc-hcp energy difference, compared to the NM case [63]. The above results emphasize that the survived local magnetic moments play critical role in determining thermodynamics of the alloys and should be carefully considered in various alloys.

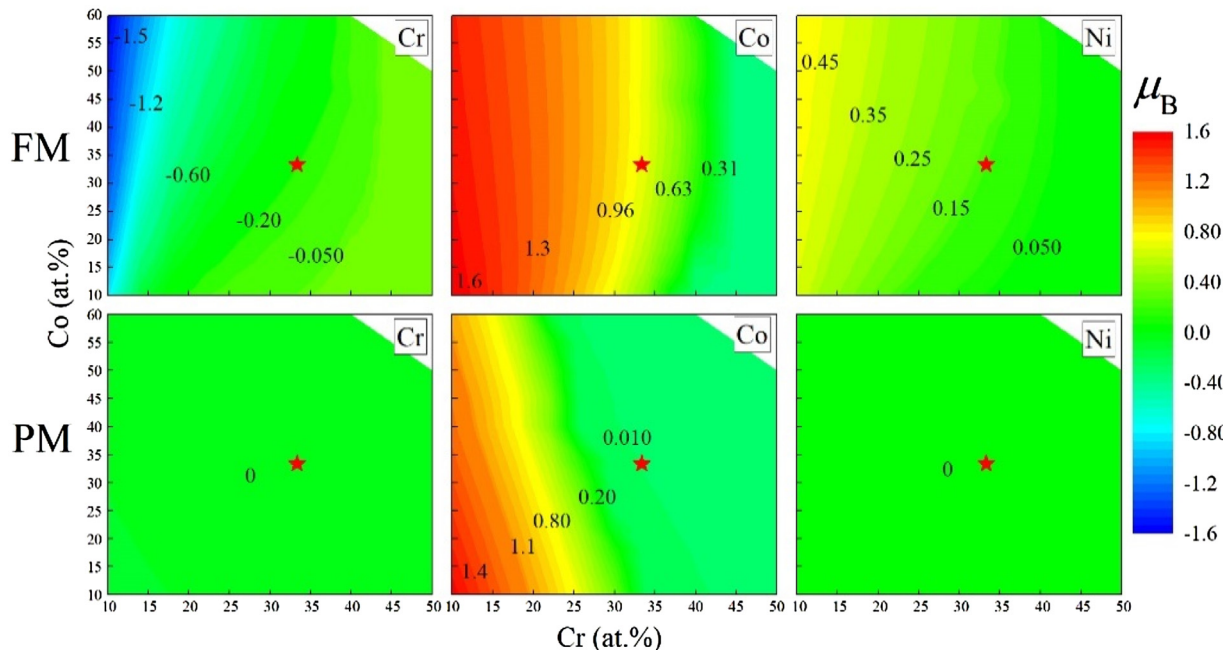


Fig. 4. The local magnetic moments (in units of μ_{B}) on various atoms for the FM (upper panel) and PM (lower panel) states. The position corresponding to the CrCoNi MEA is indicated by a red star.

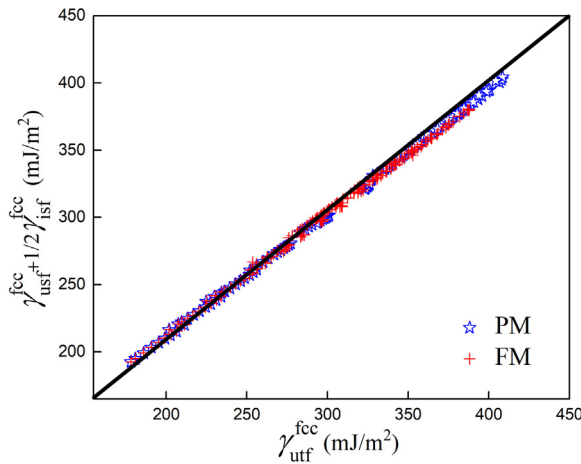


Fig. 5. Universal scaling law in ternary Cr-Co-Ni alloys at both PM and FM states.

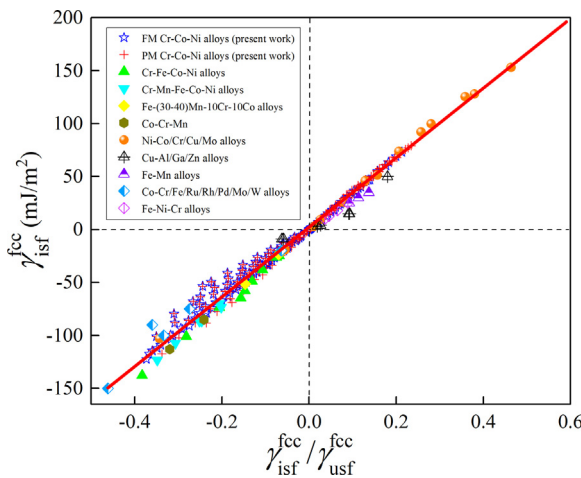


Fig. 6. The relationship between $\gamma_{\text{isf}}^{\text{fcc}}$ and $\gamma_{\text{isf}}^{\text{fcc}} / \gamma_{\text{usf}}^{\text{fcc}}$ for various metals and alloys. Results from current work are indicated by the symbol of blue star and red cross. Other data from Refs. [13,43,78–83] are included.

3.3. Generalized stacking fault energy and universal relations

Fig. 2(e–h) shows the maps of $\gamma_{\text{usf}}^{\text{fcc}}$ and $\gamma_{\text{utf}}^{\text{fcc}}$ for the two magnetic states. In contrast to the strong variations observed in the case of $\gamma_{\text{isf}}^{\text{fcc}}$, $\gamma_{\text{usf}}^{\text{fcc}}$ shows a much weaker chemistry dependence. $\gamma_{\text{utf}}^{\text{fcc}}$ decreases strongly with increasing Cr concentration, but barely changes with Co addition for both magnetic states. In pure metals and binary alloys, previous studies showed that the calculated GSFEs follow the universal scaling law [78,79], namely, $\gamma_{\text{utf}}^{\text{fcc}} \approx \gamma_{\text{usf}}^{\text{fcc}} + 1/2\gamma_{\text{isf}}^{\text{fcc}}$. In Fig. 5, we analyze the FM and PM GSFEs in the same way and show that the scaling law is also obeyed for both magnetic states, indicating that such a relation is dominated by the structural characteristics of the stacking fault. We mention that when segregation to stacking fault (Suzuki effect) occurs such a relation is not expected to hold [78].

The universal scaling law indicates that the energy barriers for stacking fault and twinning nucleation are not independent quantities. In fact, the stable and unstable stacking fault energies, $\gamma_{\text{isf}}^{\text{fcc}}$ and $\gamma_{\text{usf}}^{\text{fcc}}$, may also be correlated. In Fig. 6, we plot the relationship between $\gamma_{\text{isf}}^{\text{fcc}}$ and $\gamma_{\text{isf}}^{\text{fcc}} / \gamma_{\text{usf}}^{\text{fcc}}$ for various alloy systems [13,43,78–83]. $\gamma_{\text{isf}}^{\text{fcc}} / \gamma_{\text{usf}}^{\text{fcc}}$ can be considered as a characteristic material parameter [79]. Approximately, for each alloy systems, linear correlation between $\gamma_{\text{isf}}^{\text{fcc}}$ and $\gamma_{\text{isf}}^{\text{fcc}} / \gamma_{\text{usf}}^{\text{fcc}}$ exists, which holds in both stable and metastable systems with positive or negative stacking fault energies. Theoretically, twinning nucleation and growth

should be governed by the whole γ -surface including the stable formation energy ($\gamma_{\text{isf}}^{\text{fcc}}$) and the energy barriers ($\gamma_{\text{usf}}^{\text{fcc}}$ and $\gamma_{\text{utf}}^{\text{fcc}}$) [43]. For instance, Asaro and Suresh [84] proposed that the twinnability of fcc materials can be measured by a parameter T , defined by

$T = \sqrt{(3\gamma_{\text{usf}}^{\text{fcc}} - 2\gamma_{\text{isf}}^{\text{fcc}}) / \gamma_{\text{utf}}^{\text{fcc}}}$. They argued that deformation twinning is favored for $T > 1$, while dislocation slip for $T < 1$. Similarly, Jo et al. [85] proposed another dimensionless parameter to classify the prevalent deformation mechanisms, $r_d = \gamma_{\text{isf}}^{\text{fcc}} / (\gamma_{\text{usf}}^{\text{fcc}} - \gamma_{\text{isf}}^{\text{fcc}})$, where twinning is preferred for low r_d values. According to the revealed relation between $\gamma_{\text{isf}}^{\text{fcc}}$ and $\gamma_{\text{isf}}^{\text{fcc}} / \gamma_{\text{usf}}^{\text{fcc}}$, those twinnability measures can be simplified to be dependent on a single parameter $\gamma_{\text{isf}}^{\text{fcc}}$. Overall, the above relations among stable and unstable stacking fault energies rationalize the empirical correlation between the SFE and the deformation modes, namely, twinning correlates with low SFE.

4. Discussion

The physical and mechanical behaviors of ternary Cr-Co-Ni alloys possess strong chemical dependence [13,65], which stresses the importance of computation-aided designing as proposed in the present work. Based on the obtained composition and magnetism dependent maps of SFE (Fig. 2), one may understand better the composition dependent deformation behaviors in various ternary Cr-Co-Ni alloys [13] and design new alloys with desired deformation mechanisms. In the following we use the equiatomic CrCoNi MEA as a reference alloy for discussing the composition-dependent deformation mechanism in non-equiatomic TRIP/TWIP Cr-Co-Ni MEAs.

4.1. FM high-Co low-Cr alloys

High-Co concentration leads to high T_c , and these alloys are usually FM at room or cryogenic temperatures. As predicted in Fig. 2(c), for a fixed Cr concentration, the primary deformation mode changes from TW to deformation-induced martensitic transformation (DIMT) with increasing Co concentration, which is in perfect agreement with the observations made by Remy and Pineau [13] in the ternary $\text{Cr}_{15}\text{Co}_{75-x}\text{Ni}_x$ ($20 \leq x \leq 35$, T3-T6 marked in Fig. 2(c)) alloys. They further showed that decreasing temperature can induce the deformation mode transition from deformation twins (DT) to DIMT. In fact, according to Fig. 2(c), the most efficient way in tuning the SFE is changing Cr and Co concentrations simultaneously.

Particularly, when following a route approximately along the constant-SFE line in Fig. 2(c), it is predicted that the PM CrCoNi MEA and the FM $\text{Cr}_{15}\text{Co}_{50}\text{Ni}_{35}$ alloy (T4 alloy in Ref. [13]) should deform in a similar way (similar SFE), which is indeed confirmed by experiments [4,13]. Consequently, these two alloys possess very similar tensile strength and ductility since they both deform by prevalent twinning and their twinnabilities are predicted similar, as well as the temperature dependence [4,6,13]. Furthermore, from Fig. 2(a) and (c) we see that $\text{Cr}_{15}\text{Co}_{40}\text{Ni}_{45}$ (T6 alloy in Ref. [13]) is more stable than the reference CrCoNi MEA, and accordingly its twinnability should be weaker. Indeed, it was observed that when $\text{Cr}_{15}\text{Co}_{40}\text{Ni}_{45}$ is deformed at 300 K and 77 K, twinning starts at around 30% and 10% strains, respectively; both are larger than the critical strains (12.9% at 300 K and 6.7% at 77 K) in CrCoNi MEA [68]. Further notice that $\text{Cr}_{15}\text{Co}_{55}\text{Ni}_{30}$ (T3, $T_c = 385$ K [13]) has the best ductility among T3-T6 alloys at room temperature but its ductility gradually decreases with decreasing temperature. This is due to the fact that decreasing temperature promotes the tendency of MT by decreasing the SFE, and the increasing fraction of mechanically ε -martensite deteriorates ductility. The above comparison between FM and PM alloys may imply that magnetism affects the deformation mechanism and

plastic properties in an indirect way, i.e., through its effects on thermodynamic stability and SFEs.

4.2. PM low-Co high-Cr alloys

High-Cr and low-Co concentrations quickly decrease T_c , therefore these alloys are examined at the PM state (Fig. 2(d)). It is important to observe that the constant $\gamma_{\text{isf}}^{\text{fcc}}$ line at the PM state differ notably from those at the FM one. As an example, for the same Ni concentration, Cr₂₀Co₄₀Ni₄₀, Cr₃₀Co₃₀Ni₄₀ and Cr₄₀Co₂₀Ni₄₀ alloys have different $\gamma_{\text{isf}}^{\text{fcc}}$ values, thereby different twinnability at the PM state; while at the FM state they all have very similar $\gamma_{\text{isf}}^{\text{fcc}}$ values. Future experiments are needed to study the mechanical properties and deformation mechanisms in these alloys.

Yoshida et al. [65] studied the effect of Co content on the deformation mechanism in Cr₄₀Co₂₀Ni₄₀, Cr₃₀Co₄₀Ni₃₀ and Cr₂₀Co₆₀Ni₂₀ alloys. In Cr₄₀Co₂₀Ni₄₀, tiny amount of ε -martensite (0.4 %) was observed in the fractured specimen, indicating the metastability of the alloy. In Cr₃₀Co₄₀Ni₃₀, DT was the dominant deformation mechanism at early strains and ε -martensite was observed at later stages of deformation. ε -martensite increases gradually from 0.9 % at 38 % strain to 11 % at fracture strain 53 %, accompanying with more deformation twins. Both Cr₄₀Co₂₀Ni₄₀ and Cr₃₀Co₄₀Ni₃₀ are PM at room temperature. The above observations agree perfectly with the present predictions in Fig. 2(b) and (d) showing that Cr₃₀Co₄₀Ni₃₀ is less stable than Cr₄₀Co₂₀Ni₄₀ and both have negative $\gamma_{\text{isf}}^{\text{fcc}}$ and γ_0^{fcc} . While in Cr₂₀Co₆₀Ni₂₀, the fraction of ε -martensite quickly increases to 43 % at fracture. Note that Cr₂₀Co₆₀Ni₂₀ is FM at room temperature (Fig. 1(a)). From Fig. 2(a) and (c), one can see that this alloy is less stable than alloy T3–Cr₁₅Co₅₅Ni₃₀. Therefore, the observed early formation of ε -martensite in Cr₂₀Co₆₀Ni₂₀ is consistent with the previous results by Remy and Pineau [13], which is also in nice agreement with our calculations. We emphasize that PM SFE of Cr₂₀Co₆₀Ni₂₀ (or NM result) in Fig. 3 would result in misleading conclusions, compared to those for Cr₄₀Co₂₀Ni₄₀ and Cr₃₀Co₄₀Ni₃₀.

Additionally, at the high-Cr corner in Fig. 2(d), the SFE shows week dependence on Cr content, which may give us more freedom to adjust the combination of yield strength and ductility. For example, it was suggested that Cr atoms in the ternary Cr–Co–Ni alloys lead to higher level of local lattice distortion and thereby cause higher friction stress against dislocation movement [86,87]. Therefore, it is speculated that increasing Cr concentration while maintaining the TWIP/TRIP effects through adjusting Co concentration may lead to high yield strength and high ductility simultaneously. Indeed, recently experiments show that compared to the CrCoNi MEA, the Cr₄₀Co₂₀Ni₄₀ or Cr₄₅Ni_{27.5}Co_{27.5} alloys show higher yield strengths while maintaining similar levels of ductility [65,86,87].

4.3. PM high-Co high-Cr alloys

Since both Cr and Co additions decrease the stability of the fcc solid solutions, the high-Co high-Cr alloys in this composition region have even smaller $\gamma_{\text{isf}}^{\text{fcc}}$ and γ_0^{fcc} compared to the CrCoNi MEA. Note that macroscopically the CrCoNi MEA deforms predominantly by DT and shows the typical TWIP effect [68]. By simultaneously increasing Co and Cr contents, the hcp phase quickly becomes more stable than the fcc one and we expect more DIMT and therefore the TRIP effect.

Furthermore, there may also exist the thermally induced hcp phase, realizing the hcp+fcc dual-phase microstructure in the as-quenched state when enough Co and Cr are added. As previ-

ously demonstrated in the quaternary Cr–Mn–Fe–Co alloys, with decreasing Mn concentration, i.e., decreasing the stability of the fcc structure and the $\gamma_{\text{isf}}^{\text{fcc}}$, the microstructure changes from the single fcc phase to the fcc+hcp dual-phase, which enables the TRIP-assisted dual-phase design in the Cr₁₀Mn₃₀Fe₅₀Co₁₀ HEA [10]. In the binary Co–Cr alloys with 85–70 at.% Co the area fraction of hcp in the quenched specimens was found more than 80 % [57] and the martensitic start temperature (M_s) for the fcc→hcp phase transformation is about 750–1000 °C [88]; while in the binary Co–Ni alloys, M_s quickly decreases below the room temperature for the Ni concentration higher than ~30 at.% [46] and the martensitic transformation is remarkably sluggish [89,90]. Therefore, further experiments are needed to find out at which composition/temperature the thermally induced hcp martensite occurs in the ternary alloys and its effect on the tensile properties. In the quinary Cr–Mn–Fe–Co–Ni alloys, the hcp+fcc dual-phase structure has been successfully realized by increasing Co content and reducing the concentrations of the austenite stabilizing elements, e.g., Ni and Mn [57,91]. For example, starting from the CrMnFe–CoNi HEA, Liu et al. [67] showed that increasing Co concentration to more than 27 at.%, compensated by the reduction in Ni content, leads to the occurrence of thermally induced hcp phase. Importantly, it results in a continuous improvement in both strength and ductility with increasing Co content by enhancing the TWIP effect and/or triggering the TRIP effect [67]. Similar design strategy has been adopted by Wang et al. [57] and Wei et al. [91] in this quinary HEA system, but with different concentration combinations, as well as in the quaternary Cr–Fe–Co–Ni alloys [92]. In principle, there are infinite ways to tailor the composition in the multiple component alloys, but the thermodynamic driving force should play a crucial role in affecting the fraction of the thermally induced hcp phase f_{hcp} . Wang et al. [57] argued that in the quinary Cr–Mn–Fe–Co–Ni alloys, f_{hcp} may be described by the Johnson–Mehl–Avrami–Kolmogorov type of expression in thermodynamic calculations, $f_{\text{hcp}} = 1 - \exp \left[k \left(\frac{D_m}{RT} \right)^n \right]$, where k and n are fitting parameters, D_m is the calculated driving force, which is strongly related to γ_0^{fcc} (or $\Delta F_{\text{fcc}-\text{hcp}}$), R is the gas constant and T is the absolute temperature [57]. The above studies precisely emphasize the pressing demand of the theoretical studies as presented in the present work to save the experimental effort to seek for optimized alloys with desired phases and strengthening mechanisms.

4.4. FM/PM low-Co low-Cr alloys

In this region, alloys have thermodynamically stable fcc phase ($\gamma_{\text{isf}}^{\text{fcc}} > 0$) due to the high content of Ni. Increasing the $\gamma_{\text{isf}}^{\text{fcc}}$ by decreasing Cr and/or Co concentrations will suppress DT and weakens the TWIP effect. Therefore alloys in this region will become akin to the conventional Ni-based alloys.

5. Conclusions

Using *ab initio* alloy theory, we investigated the chemical and magnetic effects on the γ -surface of the ternary Cr–Co–Ni alloys. We found that both Co and Cr additions lower the SFE and the fcc phase stability. Particularly, the Co- and Cr-rich alloys, compared to the well-studied equiatomic CrCoNi MEA, show even more negative γ_0^{fcc} and $\gamma_{\text{isf}}^{\text{fcc}}$ values, indicating that the hcp phase is energetically more favorable than the fcc one and that the tendency of the occurrence of DIMT (or the TRIP effect) is promoted by simultaneously increasing Co and Cr concentrations. The present theoretical predictions are consistent with the available experimental observations. Our results emphasize the critical role played by magnetism

and show that the predicted deformation modes in Co-rich alloys are sensitive to the magnetic state. The obtained composition and magnetism dependent γ -surface enables us to better understand the deformation behaviors in various ternary Cr-Co-Ni alloys and facilitate future composition design/optimization of TRIP and TWIP Cr-Co-Ni MEAs.

Declaration of Competing Interest

The authors report no declarations of interest.

Acknowledgements

This work was financially supported by the Major State Basic Research Development Program of China (No. 2016YFB0701405). This work is also supported by the KTH-SJTU collaborative research and development seed grant in 2018, the Swedish Research Council (No. 2019-04971), the Swedish Foundation for Strategic Research, the China Scholarship Council, the Swedish Energy Agency, and the Hungarian Scientific Research Fund (No. research project OTKA 128229), the Fundamental Research Funds for the Central Universities (No. N180204015). The computation resource provided by the Swedish National Infrastructure for Computing (SNIC) at the National Supercomputer Centre in Linköping, which is partially funded by the Swedish Research Council through grant agreement no. 2018-05973, is acknowledged.

References

- [1] J.W. Yeh, S.K. Chen, S.J. Lin, J.Y. Gan, T.S. Chin, T.T. Shun, C.H. Tsau, S.Y. Chang, *Adv. Eng. Mater.* 6 (2004) 299–303.
- [2] B. Cantor, I.T.H. Chang, P. Knight, A.J.B. Vincent, *Mater. Sci. Eng. A* 375–377 (2004) 213–218.
- [3] B. Gludovatz, A. Hohenwarter, K.V.S. Thurston, H. Bei, Z. Wu, E.P. George, R.O. Ritchie, *Nat. Commun.* 7 (2016) 10602.
- [4] J. Miao, C.E. Slone, T.M. Smith, C. Niu, H. Bei, M. Ghazisaeidi, G.M. Pharr, M.J. Mills, *Acta Mater.* 132 (2017) 35–48.
- [5] M.S. Lucas, G.B. Wilks, L. Mauger, J.A. Munoz, O.N. Senkov, E. Michel, J. Horwath, S.L. Semiatin, M.B. Stone, D.L. Abernathy, E. Karapetrova, *Appl. Phys. Lett.* 100 (2012), 251907.
- [6] Z. Wu, H. Bei, G.M. Pharr, E.P. George, *Acta Mater.* 81 (2014) 428–441.
- [7] F. Otto, A. Dlouhý, C. Somsen, H. Bei, G. Eggeler, E.P. George, *Acta Mater.* 61 (2013) 5743–5755.
- [8] D. Ma, M. Yao, K.G. Pradeep, C.C. Tasan, H. Springer, D. Raabe, *Acta Mater.* 98 (2015) 288–296.
- [9] Z. Li, K.G. Pradeep, Y. Deng, D. Raabe, C.C. Tasan, *Nature* 534 (2016) 227.
- [10] Z. Li, C.C. Tasan, K.G. Pradeep, D. Raabe, *Acta Mater.* 131 (2017) 323–335.
- [11] I. Gutierrez-Urrutia, D. Raabe, *Acta Mater.* 59 (2011) 6449–6462.
- [12] Y. Deng, C.C. Tasan, K.G. Pradeep, H. Springer, A. Kostka, D. Raabe, *Acta Mater.* 94 (2015) 124–133.
- [13] L. Remy, A. Pineau, *Mater. Sci. Eng.* 26 (1976) 123–132.
- [14] L. Remy, A. Pineau, *Mater. Sci. Eng.* 28 (1976) 99–107.
- [15] S. Allain, J.P. Chateau, O. Bouaziz, S. Migot, N. Guelton, *Mater. Sci. Eng. A* 387–389 (2004) 158–162.
- [16] D.T. Pierce, J.A. Jimenes, J. Bentley, D. Raabe, J.E. Wittig, *Acta Mater.* 100 (2015) 178–190.
- [17] G. Laplanche, A. Kostka, O.M. Horst, G. Eggeler, E.P. George, *Acta Mater.* 118 (2016) 152–163.
- [18] B.C.D. Cooman, Y. Estrin, S.K. Kim, *Acta Mater.* 142 (2018) 283–362.
- [19] X. Sun, S. Lu, R.W. Xie, X.H. An, W. Li, T. Zhang, C.X. Liang, X.D. Ding, Y. Wang, H. Zhang, L. Vitos, *arXiv* (2005) 09983.
- [20] J.W. Bae, J.B. Seol, J. Moon, S.S. Sohn, M.J. Jang, H.Y. Um, B. Lee, H.S. Kim, *Acta Mater.* 161 (2018) 388–399.
- [21] S. Yang, M. Jiang, H. Li, Y. Liu, L. Wang, *Rare Met.* 31 (2012) 75–80.
- [22] Z. Zhang, H. Sheng, Z. Wang, B. Gludovatz, Z. Zhang, E.P. George, Q. Yu, S.X. Mao, R.O. Ritchie, *Nat. Commun.* 8 (2017) 14390.
- [23] Y.H. Zhang, Y. Zhuang, A. Hu, J.J. Kai, C.T. Liu, *Scr. Mater.* 130 (2017) 96–99.
- [24] M.B. Kivy, M.A. Zaeem, *Scr. Mater.* 139 (2017) 83–86.
- [25] L. Vitos, P.A. Korzhavyi, B. Johansson, *Phys. Rev. Lett.* 96 (2006), 117210.
- [26] F. Walsh, M. Asta, R.O. Ritchie, *arXiv* (2004) 09086.
- [27] J. Ding, Q. Yu, M. Asta, R.O. Ritchie, *Proc. Natl. Acad. Sci. U.S. A.* 115 (2018) 8919–8924.
- [28] Q.J. Li, H. Sheng, E. Ma, *Nat. Commun.* 10 (2019) 3563.
- [29] Q. Ding, Y. Zhang, X. Chen, X. Fu, D. Chen, S. Chen, L. Gu, F. Wei, H. Bei, Y. Gao, M. Wen, J. Li, Z. Zhang, T. Zhu, R.O. Ritchie, Q. Yu, *Nature* 574 (2019) 223–227.
- [30] R. Zhang, S. Zhao, J. Ding, Y. Chong, T. Jia, C. Ophus, M. Asta, R.O. Ritchie, A.M. Minor, *Nature* 581 (2020) 283–287.
- [31] E.P. George, D. Raabe, R.O. Ritchie, *Nat. Rev. Mater.* 4 (2019) 515–534.
- [32] B.C. Sales, K. Jin, H. Bei, J. Nichols, M.F. Chisholm, A.F. May, N.P. Butch, A.D. Christianson, M.A. McGuire, *Nat. Commun.* 2 (2017) 33.
- [33] L. Vitos, I.A. Abrikosov, B. Johansson, *Phys. Rev. Lett.* 87 (2001), 156401.
- [34] L. Vitos, *Phys. Rev. B* 64 (2001) 167.
- [35] P. Hohenberg, W. Kohn, *Phys. Rev. B* 136 (1964) 864.
- [36] O.K. Andersen, O. Jepsen, G. Krier, in: V. Kumar, O.K. Andersen, A. Mookerjee (Eds.), *Lectures on Methods of Electronic Structure Calculations*, ICTP, Trieste, 1992.
- [37] J.P. Perdew, K. Burke, M. Ernzerhof, *Phys. Rev. Lett.* 77 (1996) 3865.
- [38] B. Györffy, *Phys. Rev. B* 5 (1972) 2382.
- [39] B.L. Györffy, A.J. Pindor, J. Staunton, G.M. Stocks, H. Winter, *J. Phys. F Met. Phys.* 15 (1985) 1337.
- [40] Z. Dong, L. Vitos, *Scr. Mater.* 171 (2019) 78–82.
- [41] L. Vitos, J.O. Nilsson, B. Johansson, *Acta Mater.* 54 (2019) 3821–3826.
- [42] G. Laplanche, P. Gadaud, C. Bärsch, K. Demtröder, C. Reinhart, J. Schreuer, E.P. George, *J. Alloys Compd.* 746 (2018) 244.
- [43] S. Kibey, J.B. Liu, D.D. Johnson, H. Sehitoglu, *Acta Mater.* 55 (2007) 6843–6851.
- [44] B. Gan, J.M. Wheeler, Z. Bi, L. Liu, J. Zhang, H. Fu, *J. Mater. Sci. Technol.* 35 (2019) 957–961.
- [45] J.R. Thompson, A. Goyal, D.K. Christen, D.M. Kroeger, *Phys. C* 370 (2001) 169–176.
- [46] T. Nishizawa, K. Ishida, *Bull. Alloy Phase Diagr.* 4 (1983) 390–395.
- [47] D. Ma, B. Grabowski, F. Körmann, J. Neugebauer, D. Raabe, *Acta Mater.* 100 (2015) 90–97.
- [48] X.X. Wu, Z. Li, Z. Rao, Y. Ikeda, B. Dutta, F. Kormann, J. Neugebauer, D. Raabe, *Phys. Rev. Mater.* 4 (2020), 033601.
- [49] F. Körmann, D. Ma, D.D. Belyea, M.S. Lucas, C.W. Miller, B. Grabowski, M.H.F. Sluiter, *Appl. Phys. Lett.* 107 (2015), 142404.
- [50] B.C. Sales, K. Jin, H. Bei, G.M. Stocks, G.D. Samolyuk, A.F. May, M.A. McGuire, *Sci. Rep.* 6 (2016) 26179.
- [51] P. Nash, *Bull. Alloy Phase Diagr.* 7 (1986) 466–476.
- [52] K. Ishida, T. Nishizawa, *Bull. Alloy Phase Diagr.* 11 (1990) 357–370.
- [53] F. Zhang, Y. Wu, H. Lou, Z. Zeng, V.B. Prakapenka, E. Greenberg, Y. Ren, J. Yan, J.S. Okasinski, X. Liu, Y. Liu, Q. Zeng, Z. Lu, *Nat. Commun.* 8 (2017) 1–7.
- [54] C.L. Tracy, S. Park, D.R. Rittman, S.J. Zinkle, H. Bei, M. Lang, R.C. Ewing, W.L. Mao, *Nat. Commun.* 8 (2017) 15634.
- [55] F.X. Zhang, S. Zhao, K. Jin, H. Bei, D. Popov, C. Park, Y. Zhang, *Appl. Phys. Lett.* 110 (2017), 011902.
- [56] B.X. Huang, X.D. Wang, Y.H. Rong, L. Wang, L. Jin, *Mater. Sci. Eng. A* 438 (2006) 306–311.
- [57] W. Wang, Z. Hou, R. Lizárraga, Y. Tian, R.P. Babu, E. Holmstrom, H. Mao, H. Larsson, *Acta Mater.* 176 (2019) 11–18.
- [58] G.B. Olson, M. Cohen, *Metall. Trans. A* 7 (1976) 1897–1904.
- [59] R. Li, S. Lu, D. Kim, S. Schönecker, J. Zhao, S.K. Kwon, L. Vitos, *J. Phys. Condens. Matter.* 28 (2016) 39.
- [60] P.J.H. Denteneer, W. van Haeringen, *J. Phys. C* 20 (1987) 883.
- [61] R. Lizárraga, F. Pan, L. Bergqvist, E. Holmström, L. Vitos, *Sci. Rep.* 7 (2017) 3778.
- [62] M. Uhl, J. Kübler, *Phys. Rev. Lett.* 77 (1996) 334.
- [63] C. Niu, C.R. LaRosa, J. Miao, M.J. Mills, *Nat. Commun.* 9 (2018) 1363.
- [64] F. Tian, L.K. Varga, J. Shen, L. Vitos, *Comput. Mater. Sci.* 111 (2016) 350–358.
- [65] S. Yoshida, T. Ikeuchi, Y. Bai, N. Tsuji, *Mater. Trans.* 67 (2020) 113–120.
- [66] E.H. Köster, A.R. Thölen, A. Howie, *Philos. Mag.* 10 (1964) 1093–1095.
- [67] S.F. Liu, Y. Wu, H.T. Wang, J.Y. He, J.B. Liu, C.X. Chen, X.J. Liu, H. Wang, Z.P. Lu, *Intermetallics* 93 (2018) 269–273.
- [68] G. Laplanche, A. Kostka, C. Reinhart, J. Hunfeld, G. Eggeler, E.P. George, *Acta Mater.* 128 (2017) 292–303.
- [69] S. Huang, H. Huang, W. Li, D. Kim, S. Lu, X. Li, E. Holmstrom, S.K. Kwon, L. Vitos, *Nat. Commun.* 9 (2018) 2381.
- [70] S.F. Liu, Y. Wu, H.T. Wang, W.T. Lin, Y.Y. Shang, J.B. Liu, K. An, X.J. Liu, H. Wang, Z.P. Lu, *J. Alloys Compd.* 792 (2019) 444–455.
- [71] M. Chandran, S.K. Sondhi, *J. Appl. Phys.* 109 (2011), 103525.
- [72] J. Unfried-Silgado, L. Wu, F.F. Ferreira, C.M. Garzon, A.J. Ramirez, *Mater. Sci. Eng. A* 558 (2012) 70–75.
- [73] J.M. Drapier, D. Coutouradis, L. Habraken, *Acta Metall.* 15 (1967) 673–675.
- [74] E. Aerts, P. Delavignette, R. Siems, S. Amelinckx, *J. Appl. Phys.* 33 (1962) 3078–3080.
- [75] Z. Zhang, M.M. Mao, J. Wang, B. Gludovatz, Z. Zhang, S.X. Mao, E.P. George, Q. Yu, R.O. Ritchie, *Nat. Commun.* 6 (2015) 10143.
- [76] T.M. Smith, M.S. Hooshmand, B.D. Esser, F. Otto, D.W. McComb, E.P. George, M. Ghazisaeidi, M.J. Mills, *Acta Mater.* 110 (2016) 352–363.
- [77] L. Qi, C.Q. Liu, H.W. Chen, J.F. Nie, *Acta Mater.* 199 (2020) 649–668.
- [78] W. Li, S. Lu, Q.-M. Hu, S.K. Kwon, B. Johansson, L. Vitos, *J. Phys. Condens. Matter* 26 (2014), 265005.
- [79] Z.H. Jin, S.T. Dunham, H. Gleiter, H. Hahn, P. Gumbsch, *Scr. Mater.* 64 (2011) 605–608.
- [80] W. Li, S. Lu, D. Kim, K. Kokko, S. Hertzman, S.K. Kwon, L. Vitos, *Appl. Phys. Lett.* 108 (2016), 081903.
- [81] L.Y. Tian, R. Lizárraga, H. Larsson, E. Holmström, L. Vitos, *Acta Mater.* 136 (2017) 215–223.
- [82] W. Zhao, W. Li, Z. Sun, S. Gong, L. Vitos, *Mater. Des.* 124 (2017) 100–107.
- [83] Z. Dong, S. Schönecker, D. Chen, W. Li, S. Lu, L. Vitos, *Int. J. Plast.* 119 (2019) 123–139.
- [84] R.J. Asaro, S. Suresh, *Acta Mater.* 53 (2005) 3369–3382.
- [85] M. Jo, Y.M. Koo, B.J. Lee, B. Johansson, L. Vitos, S.K. Kwon, Proc. Natl. Acad. Sci. U.S.A. 111 (2014) 6560–6565.

- [86] F.G. Coury, K.D. Clarke, C.S. Kiminami, M.J. Kaufman, A.J. Clarke, *Sci. Rep.* 8 (2018) 8600.
- [87] S. Yoshida, T. Ikeuchi, T. Bhattacharjee, Y. Bai, A. Shibata, N. Tsuji, *Acta Mater.* 171 (2019) 201–215.
- [88] Z. Li, H. Mao, P.A. Korzhavyi, M. Selleby, *Calphad* 52 (2016) 1–7.
- [89] Y. Liu, H. Yang, G. Tan, S. Miyazaki, B. Jiang, Y. Liu, *J. Alloys Compd.* 746 (2018) 244.
- [90] H. Yang, Y. Liu, *Acta Mater.* 54 (2006) 4895–4904.
- [91] D. Wei, X. Li, J. Jiang, W. Heng, Y. Koizumi, W.M. Choi, B.J. Lee, H.S. Kim, H. Kato, A. Chiba, *Scr. Mater.* 165 (2019) 39–43.
- [92] W. Fang, R. Chang, P. Ji, X. Zhang, B. Liu, X. Qu, F. Yin, *Metals* 8 (2018) 369.